SUPPORTING INFORMATION

Imaging electrical resonance in hair cells

Materials and Methods

Modeling electrical resonance in frog saccular hair cells

Current flowing across an intact sensory epithelium passes through hair cells or around them. We constructed a corresponding equivalent-circuit model (Fig. 1*A*) comprising the electrical impedances of the hair cell's apical and basolateral membranes as well as the shunt impedance. The apical impedance accounted for the resistance and capacitance of the hair bundle, which were added in series to the corresponding impedance of the basolateral surface. The individual circuit element values used were as follows: leak resistance of the hair cell's apical surface, 1.0 GΩ; average conductance of the hair bundle, 0.7 nS; resistance of the hair cell's basolateral surface, 800 MΩ; shunt resistance of the epithelial sheet, 20.0 kΩ; capacitance of the hair cell's apical membrane including the hair bundle, 4.71 pF; capacitance of the hair cell's basolateral membrane, 8.64 pF, and capacitance of the shunt pathway, 3.92 nF. To account for the delayed conductance of Ca^{2+}-sensitive K^+ channels, we attributed a phenomenological inductance of 760 kH to the basolateral membrane.

We defined the impedances Z_A, Z_B, and Z_S, in which the successive subscripts correspond to the apical, basolateral, and shunt pathways:

$$Z_A = \frac{1}{\frac{1}{R_A} + i\omega C_A},$$

$$Z_B = \frac{1}{\frac{1}{R_B} + i\left(\frac{C_B}{\omega}\right)\left(\omega^2 - {\omega_0}^2\right)}, \text{ and}$$

$$Z_S = \frac{1}{\frac{1}{R_S} + i\omega C_S}.$$

Here C and R are capacitances and resistances and $\omega_0 = f_0/(2\pi)$ is the basolateral membrane's resonant frequency. When driven by sinusoidal current stimulation $I = I_0 e^{i\omega t}$ at an angular frequency ω, the voltage drops across the hair cell's apical and basolateral membranes are respectively

$$V_A = \left(\frac{-Z_A Z_S}{Z_A + Z_B + Z_S} \right) I \quad \text{and}$$

$$V_B = \left(\frac{Z_B Z_S}{Z_A + Z_B + Z_S} \right) I .$$

These voltages are complex quantities whose moduli $|V| = \sqrt{\mathrm{Re}(V)^2 + \mathrm{Im}(V)^2}$ and phase $\phi = \arg\left[\mathrm{Im}(V)/\mathrm{Re}(V)\right]$ are plotted as a function of frequency (Fig. 1*B*,*C*).

In vitro preparation of the bullfrog's sacculus

Each saccular macula was excised from an adult bullfrog (*Rana catesbeiana*) and transferred into oxygenated saline solution of osmotic strength 240 mOsmol·kg^{-1} and containing 110 mM Na^+, 2 mM K^+, 1 mM Ca^{2+}, 118 mM Cl^-, 3 mM D-glucose, and 5 mM HEPES at pH 7.3. The otolithic membrane was carefully removed after first lifting its edge with an eyelash. In experiments featuring enzymatic digestion, the excised sacculus was incubated at room temperature for 20 min in saline solution supplemented with 50 μg/ml proteinase type XXIV (Sigma-Aldrich) before removal of the otolithic membrane. When appropriate, iberiotoxin was used at a concentration of 100 nM in saline solution.

After removal of the otolithic membrane, the sacculus was centered, apical surface downward, over a 1.2 mm hole at the center of a 12 mm circular disk cut from a plastic coverslip. The periphery of the sacculus was then glued to the disk with cyanoacrylate adhesive (Iso-Dent, Ellman Instruments, Oceanside, NY). While the mounted sacculus floated on the surface of saline solution in a Petri dish, the macula was stained for 20 min with a 100 μl drop of saline solution containing 50 μg/ml of the potentiometric dye di-3-ANEPPDHQ (Invitrogen, Carlsbad, CA) in 0.5% ethanol. After staining, the disk was rinsed to remove unbound dye.

Although our measurements were not affected by fast, stimulus-evoked motion artifacts, the mounted sacculus did exhibit slow drift at approximately 10 μm per hour in both the lateral and the vertical direction. To obtain satisfactory images, we found it necessary to eliminate this drift by encasing both sides of the preparation in low-melting-point agarose (type VII-A, Sigma-Aldrich) cooled to room temperature. We deposited a drop of 3% agarose on the basal aspect of the sacculus and placed a drop of 1% agarose on the apical surface. The disk was then mounted as a partition separating two fluid-filled compartments in a recording chamber. The disk was mounted so that the surface of the sensory epithelium faced upward, toward the microscope objective (Fig. S1*A*).

Electrical stimulation

To evoke electrical resonance in hair cells, we passed a sinusoidal current of ±0.5 μA across the entire saccular epithelium. The current was provided by a constant-current source (A395, World Precision Instruments, Sarasota, FL) that was modulated by a sinusoidal voltage waveform. The current was delivered to the preparation through Ag-AgCl electrodes placed in each chamber. The voltage established across the saccular macula was monitored with a high input-impedance differential amplifier (AM 502, Tektronix, Beaverton, OR). To protect the sensory epithelium from the voltage transients that occurred when the current source was turned on or connected to the preparation, we connected a 440 mF capacitor in parallel with the preparation. The capacitor was switched out of the circuit before sinusoidal stimulation commenced.

Fluorescence imaging

For fluorescence excitation, we directed collimated 530 nm light from a 130 mW light-emitting diode array (LEDC16, Thorlabs, Newton, NJ) to the sample through the epi-illumination port of an upright microscope (Zeiss Axioskop 2, MPS Zeiss, Thornwood, NY; Fig. S1*B*). Current was provided by a programmable, rapidly switched source (S4000, Advanced Illumination, Rochester, VT) that delivered distortion-free square pulses of durations as brief as 1 μs. The

green excitation light was filtered through a narrow bandpass interference filter (530 ± 5 nm) and directed toward the preparation by a dichroic mirror with a cutoff wavelengh of 555 nm (Chroma Technology, Bellows Falls, VT). Excitation illumination was concentrated and fluorescence emission was collected by a 20X water-immersion objective lens of numerical aperture 0.95 (XLUMPlanFl, Olympus America, Hauppauge, NY). The fluorescence emission was filtered by a long-pass absorption filter (OG590, Chroma Technology, Bellows Falls, VT), demagnified 0.63X to provide a field of view encompassing the entire sensory epithelium, and focused onto a 16-bit charge-coupled-device camera with an average readout noise of 6 e^- (Orca R2, Hamamatsu Photonics, Shizuoka, Japan). Strobed illumination, electrical stimulation, and image acquisition were controlled by custom LabVIEW software (National Instruments, Austin, Texas).

Stroboscopic video microscopy and data analysis

To visualize the fluorescence signal from the sacculus over the course of a single period of sinusoidal electrical stimulation, we acquired fluorescence images with illumination pulses at specific phase delays with respect to the stimulus waveform (Fig. S1*C*). One acquired frame thus represented the fluorescence intensity pattern from illumination over a particular phase range in the stimulus cycle. Because significant signal integration was needed to overcome shot noise, the signal in each frame required the delivery of numerous illumination pulses.

The on:off duty cycle of the illumination pulses was 1:8 and the total number of pulses per frame was adjusted so that the baseline fluorescence values approached, but avoided, camera saturation. The order in which different phases were sampled was randomized to avoid systematic artifacts. For each stimulus frequency assayed, all eight phases were imaged 64 times apiece. Each of these trials included a control during which the preparation was imaged at the same phase but no electrical stimulus was delivered. Prior to averaging, this background fluorescence image was subtracted from the same trial's stimulus-evoked fluorescence image to yield 64 images at each phase representing the fluorescence attributable to the electrical stimulus.

These images were averaged and assembled into a single eight-frame stacks. One additional frame, a second measurement at the initial phase, was appended to the image stack to improve the fitting of data over a complete sinusoidal cycle. All data processing was performed with Matlab (MathWorks, Natick, MA).

The fluorescence signal from each pixel in the resulting image stack was fit to the function $F(t) = A + Bt + C \cdot \cos(t) + D \cdot \sin(t)$. The coefficients C and D could be used to deduce the amplitude of a phase-shifted sinusoidal component, $E \cdot \sin(t + \phi) = C \cdot \cos(t) + D \cdot \sin(t)$, in which $E = \sqrt{C^2 + D^2}$ and $\phi = \arctan(C/D)$. The amplitude E of a phase-shifted sinusoid was used as a thresholding parameter for statistical analysis. Although the linear term of $F(t)$ is not orthogonal to the sine and cosine terms, inclusion of this term, whose fitted amplitude was typically negligible, did not bias the extracted amplitude or phase.

Because images were acquired with high spatial resolution, our experiments yielded a large amount of data; only a small fraction of this data, however, lay in the temporal dimension. Stroboscopic imaging ultimately yielded a small number of cycles of raw data for each pixel in the field of view. Although Fourier analysis of periodic data would potentially have yielded values for the amplitude and phase that were less noisy than those extracted with a least-squares fit, the paucity of data cycles compounded with sparse temporal sampling diminished this advantage. Moreover, the large amount of raw data would have necessitated an impractically long processing time had we not averaged the data prior to analysis.

Sinusoidal fluorescence activity could be observed in the stack of eight fluorescence intensity images. To compare the amplitude of the fluorescence signal between different stimulus frequencies, we identified the frame representing the peak relative fluorescence ($\Delta F/F$) at each frequency. For each of eight phase images, the relative fluorescence was defined as the difference in fluorescence activity with respect to an initial reference frame, divided by the same reference frame.

To quantify the evidence for electrical resonance in the averaged images, we analyzed the two-dimensional standard deviation in values of the response phase. High-frequency spatial

fluctuations in the phase were first removed by applying a 3×3-pixel sliding-window average to each image. Least-squares fitting for each experiment then yielded a single image depicting the phase. After discarding pixels outside the saccular macula, we employed Matlab's Image Processing Toolbox function *stdfilt.m* to generate an image in which each pixel represented the standard deviation of the phase within a 3×3-pixel analysis window centered on the corresponding pixel in the original phase image. After generating a histogram counting all pixels in this local standard-deviation image, we quantified the fraction of the histogram's area that was bounded by the histogram envelope integrated from a standard deviation of 0 through a value of $\pi/5$. The standard-deviation histograms were by rule multimodal and featured local maxima at nearly identical locations across all experiments. Integrating the area through $\pi/5$ therefore fairly quantified the height of the lowest standard-deviation peak.

No spatial averaging was employed in mean phase calculations and log-likelihood analyses. Analysis of circular statistical data was aided by functions from the Circular Statistics Toolbox for Matlab (1). Unimodal probability-density functions were described by the von Mises distribution

$$f(\theta) = \frac{1}{2\pi I_0(\kappa)} e^{\kappa \cos(\theta - \mu)} \text{ for } 0 \le \theta \le 2\pi,$$

in which μ is the mean, κ the dispersion, and $I_0(\kappa)$ is the modified Bessel function of the first kind and order zero. Unimodal fits to the data were obtained through maximum-likelihood estimation of the mean and dispersion. For bimodal probability-density functions, we assumed a five-parameter sum of two von Mises distributions,

$$f(\theta) = p\frac{1}{2\pi I_0(\kappa_1)} e^{\kappa_1 \cos(\theta - \mu_1)} + (1-p)\frac{1}{2\pi I_0(\kappa_2)} e^{\kappa_2 \cos(\theta - \mu_2)}$$

in which *p* describes the relative proportions of the two populations. Because the convergence of maximum-likelihood estimates of the parameters for such bimodal models is highly sensitive to initial conditions (2, 3), the method is unattractive for serial comparison of noisy data sets. We therefore employed a method-of-moments procedure that used six estimating equations to solve for the five parameters (2). This procedure reliably yielded models that matched the visual

features of datasets while leaving fixed the initial parameter estimates of $\mu_1 = \pi/2$, $\mu_2 = 3\pi/2$, $\kappa_1 = 1$, and $\kappa_2 = 1$.

To determine whether the data were better described by a unimodal or a bimodal probability-density function, we compared the likelihoods that, given the data, each model would have led to that observation. The likelihood is essentially the probability of the observation given a particular underlying model. For binned histogram data, we considered a model's discrete probability density function $P(\phi) = P_1, P_2, ..., P_N$, in which N is the number of bins used for the data histogram. This function gives the probability of observing a particular phase. The likelihood, or probability that a dataset tabulated in a binned histogram would have been observed given $P(\phi)$, is

$$L = \prod_{i=1}^{N} P_i^{n_i},$$

in which n_i is the number of counts in the i^{th} bin of the histogram. The log-likelihood is therefore

$$\ln(L) = \sum_{i=1}^{N} n_i \cdot \ln(P_i).$$

As a standard for selecting models we employed an information criterion (4) that balances a model's maximized log-likelihood with its relative complexity. According to this criterion, model a is preferable to model b if

$$\ln\left(\frac{m_a}{m_b}\right) > k_a - k_b,$$

in which m_a and m_b are the maximum-likelihood estimates of models a and b, and k_a and k_b are the number of parameters in the respective models. Because maximum-likelihood estimation did not reliably converge on reasonable parameters for a bimodal model, we computed the likelihood for that model with parameters from the method-of-moments procedure. This likelihood was compared to the maximum-likelihood estimate of a unimodal model to provide a metric for bimodality. Because the parameters for the bimodal model were selected using a different method from that used for the unimodal model, datasets that appeared purely unimodal occasionally yielded a slightly higher log-likelihood for a unimodal than for a bimodal model.

Because a unimodal von Mises function is simply a subset of bimodal von Mises functions, the unimodal model should in theory never be preferable.

1. Berens P (2009) CircStat: A MATLAB toolbox for circular statistics. *J Stat Software* **31,** 1-21.
2. Jones TA (2006) MATLAB functions to analyze directional (azimuthal) data-I: Single-sample inference. *Comput Geosci* **32,** 166-175.
3. Jones TA, James, W.R. (1969) Analysis of bimodal orientation data. *Math Geol* **1,** 129-135.
4. Akaike H (1974) A new look at the statistical model identification. *IEEE Trans Autom Control* **19,** 716-723.

Fig. S1. Experimental apparatus and measurement protocol. (*A*) As shown in a cross-sectional diagram of the recording chamber, the saccular epithelium was mounted between two liquid-filled compartments, each equipped with an electrode to pass transepithelial stimulus current. (*B*) The optical system featured a bright, rapidly switched light-emitting diode (LED) that transiently illuminated the specimen during a specific phase of electrical stimulation. Fluorescence from the voltage-sensitive dye passed through the dichroic mirror to a charge-coupled-device camera (CCD). *Inset*: In response to membrane-potential changes, the emission and excitation spectra of di-3-ANEPPDHQ shifted in the indicated directions. (*C*) Three command waveforms synchronized stroboscopic imaging with electrical stimulation. Positive pulses controlled the camera's electronic shutter and thus determined the integration time for each image. During the camera's integration period, a series of current pulses to the light-emitting diode illuminated the sample at a particular phase of the sinusoidal electrical stimulus. The order in which different phases were scanned was randomized. The number of stimulus cycles over which the fluorescence was integrated varied linearly with stimulus frequency: two cycles provided a robust fluorescence signal at 25 Hz, whereas twelve cycles were required at 150 Hz. The entire paradigm was repeated 64 times to yield the average response, then reiterated without stimulation to produce a background image.

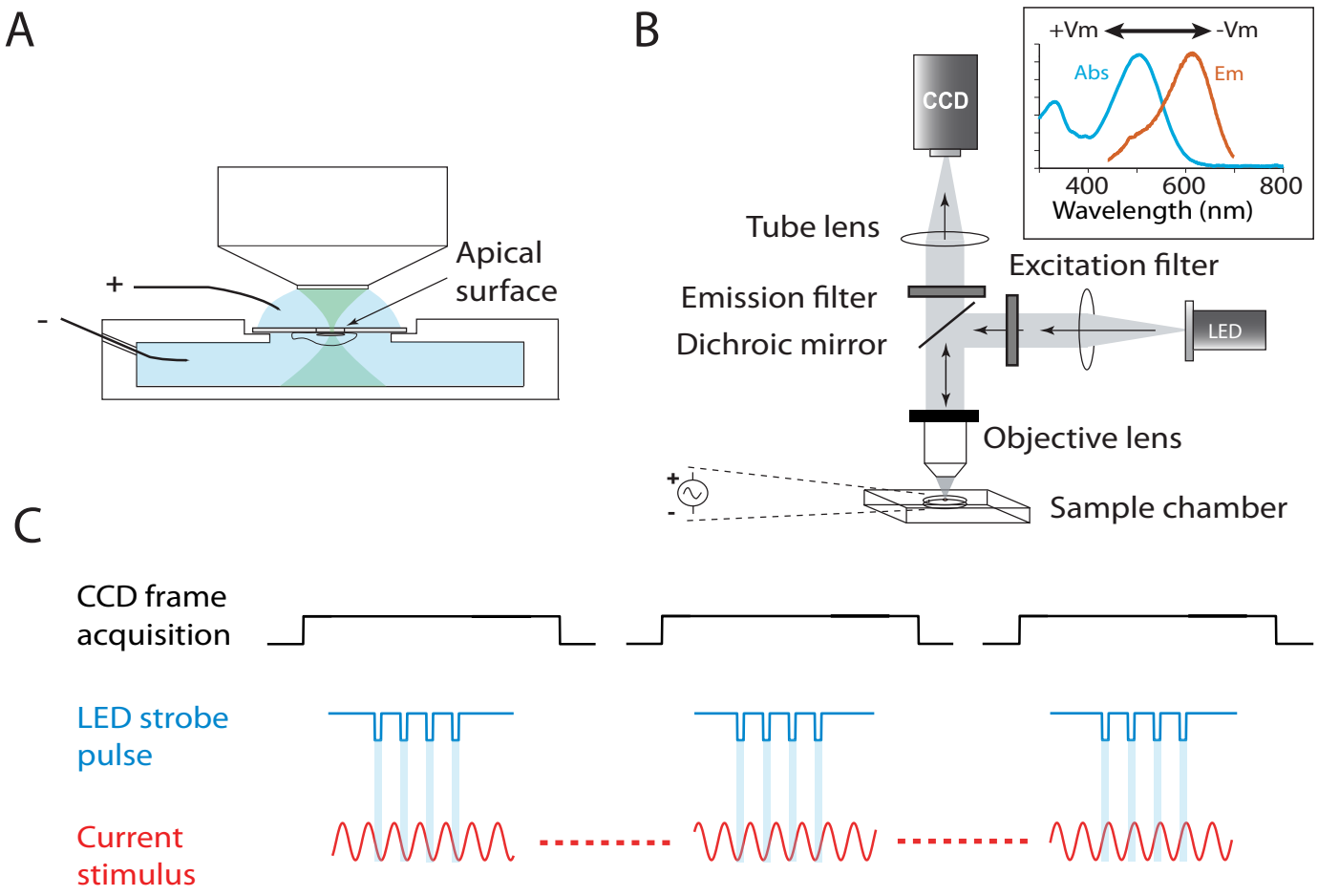
A
+
-
Apical
surface
B
CCD
+Vm
-Vm
Abs
Em
400
600
800
Wavelength (nm)
Tube lens
Excitation filter
Emission filter
Dichroic mirror
LED
Objective lens
Sample chamber
C
CCD frame
acquisition
LED strobe
pulse
Current
stimulus